J|A|C|S
ARTICLES
Published on Web 03/20/2007

Iron(III) Complex of a Crown Ether−Porphyrin Conjugate and Reversible Binding of Superoxide to Its Iron(II) Form

Katharina Dürr,[†,‡] Brendan P. Macpherson,[†] Ralf Warratz,[§] Frank Hampel,[‡] Felix Tuczek,[§] Matthias Helmreich,[‡] Norbert Jux,*[,‡] and Ivana Ivanović-Burmazović*[,†]

Contribution from the Institute of Inorganic Chemistry, University of Erlangen-Nürnberg, Egerlandstrasse 1, 91058 Erlangen, Germany, Institute of Organic Chemistry, University of Erlangen-Nürnberg, Henkestrasse 42, 91054 Erlangen, Germany, and Institute of Inorganic Chemistry, Christian-Albrechts-University Kiel, Otto Hahn Platz 6/7, 24098 Kiel, Germany

Received July 13, 2006; E-mail: ivana.ivanovic@chemie.uni-erlangen.de; norbert.jux@chemie.uni-erlangen.de

Abstract: The synthesis and characterization of the Fe(III) complex of a novel crown ether−porphyrin conjugate, 5^2-*N*-(4-aza-18-crown-6)methyl-5^4,10^4,15^4,20^4-tetra-*tert*-butyl-5^6-methyl-5,10,15,20-tetraphenylporphyrin (H_2Porph), as well as the corresponding hydroxo, dimeric, Fe(II), and peroxo species are reported. The crystal structure of $[Fe^{III}(Porph)Cl]\cdot H_3O^+\cdot FeCl_4^-\cdot C_6H_6\cdot EtOH$ is also reported. $[Fe^{III}(Porph)(DMSO)_2]^+$ and $K[Fe^{III}(Porph)(O_2^{2-})]$ are high-spin species (Mössbauer data: $\delta = 0.38$ mm s^{-1}, $\Delta E_q = 0.83$ mm s^{-1} and $\delta = 0.41$ mm s^{-1}, $\Delta E_q = 0.51$ mm s^{-1}, respectively), whereas in a solution of reduced $[Fe^{III}(Porph)(DMSO)_2]^+$ complex the low-spin $[Fe^{II}(Porph)(DMSO)_2]$ ($\delta = 0.44$ mm s^{-1}, $\Delta E_q = 1.32$ mm s^{-1}) and high-spin $[Fe^{II}(Porph)(DMSO)]$ ($\delta = 1.27$ mm s^{-1}, $\Delta E_q = 3.13$ mm s^{-1}) iron(II) species are observed. The reaction of $[Fe^{III}(Porph)(DMSO)_2]^+$ with KO_2 in DMSO has been investigated. The first reaction step, involving reduction to $[Fe^{II}(Porph)(DMSO)_2]$, was not investigated in detail because of parallel formation of an Fe(III)−hydroxo species. The kinetics and thermodynamics of the second reaction step, reversible binding of superoxide to the Fe(II) complex and formation of an Fe(III)−peroxo species, were studied in detail (by stopped-flow time-resolved UV/vis measurements in DMSO at 25 °C), resulting in $k_{on} = 36\,500 \pm 500$ M^{-1} s^{-1}, $k_{off} = 0.21 \pm 0.01$ s^{-1} (direct measurements using an acid as a superoxide scavenger), and $K_{O_2^-} = (1.7 \pm 0.2) \times 10^5$ (superoxide binding constant kinetically obtained as k_{on}/k_{off}), $(1.4 \pm 0.1) \times 10^5$, and $(9.0 \pm 0.1) \times 10^4$ M^{-1} (thermodynamically obtained in the absence and in the presence of 0.1 M NBu_4PF_6, respectively). Temperature-dependent kinetic measurements for k_{on} (−40 to 25 °C in 3:7 DMSO/CH_3CN mixture) yielded the activation parameters $\Delta H^{\ddagger} = 61.2 \pm 0.9$ kJ mol^{-1} and $\Delta S^{\ddagger} = +48 \pm 3$ J K^{-1} mol^{-1}. The observed reversible binding of superoxide to the metal center and the obtained kinetic and thermodynamic parameters are unique. The finding that fine-tuning of the proton concentration can cause the Fe(III)−peroxo species to release O_2^- and form an Fe(II) species is of biological interest, since this process might occur under very specific physiological conditions.

Introduction

The biochemistry of dioxygen and its reduced forms (O_2^- and O_2^{2-}) is closely related to that of iron−porphyrin centers in different hemoproteins. Iron(III)−superoxo and iron(III)−peroxo species are involved, for example, in the transport of dioxygen, the catalytic cycle of the monooxygenase enzyme cytochrome P450, and heme−copper assemblies.[1−5] Some iron−porphyrin complexes possess superoxide dismutase (SOD) activity and have been studied for their possible therapeutic applications.[6,7] In general, the biological relevance of the iron−porphyrins and superoxide radical anion makes the investigation of their chemical reactions deservedly attractive.

It is well established that, in aprotic coordinating solvents (e.g., dimethyl sulfoxide (DMSO) or MeCN), 1 equiv of KO_2 reduces Fe(III)−porphyrins to Fe(II), whereas an additional equivalent of KO_2 produces an Fe(III)−peroxo−porphyrin species (Scheme 1).[8,9]

Scheme 1

$$[Fe^{III}(porphyrin)]^+ + O_2^- \rightarrow [Fe^{II}(porphyrin)] + O_2 \quad (1)$$

$$[Fe^{II}(porphyrin)] + O_2^- \rightarrow [Fe^{III}(porphyrin)(O_2^{2-})]^- \quad (2)$$

Fe(III)−peroxo−porphyrin complexes comprising ligands of different electronic properties were extensively investigated by Valentine et al.[10,11] as synthetic analogues of intermediates that might occur during enzymatic reactions. All these complexes

[†] Institute of Inorganic Chemistry, University of Erlangen-Nürnberg.
[‡] Institute of Organic Chemistry, University of Erlangen-Nürnberg.
[§] Institute of Inorganic Chemistry, Christian-Albrechts-University Kiel.

(1) Momenteau, M.; Reed, C. A. *Chem. Rev.* **1994**, *94*, 659−598.
(2) Schlichting, I.; Berendzen, J.; Chu, K.; Stock, A. M.; Maves, S. A.; Benson, D. E.; Sweet, R. M.; Ringe, D.; Petsko, G. A.; Sligar, S. G. *Science* **2000**, *287*, 1615−1622.
(3) Jensen, K. P.; Ryde, U. *J. Biol. Chem.* **2004**, *279*, 14561−14569.
(4) Wertz, D. L.; Valentine, J. S. *Struct. Bonding (Berlin)* **2000**, *97*, 37−60.
(5) Kim, E.; Chufan, E. E.; Kamaraj, K.; Karlin, K. D. *Chem. Rev.* **2004**, *104*, 1077−1133.

Scheme 2

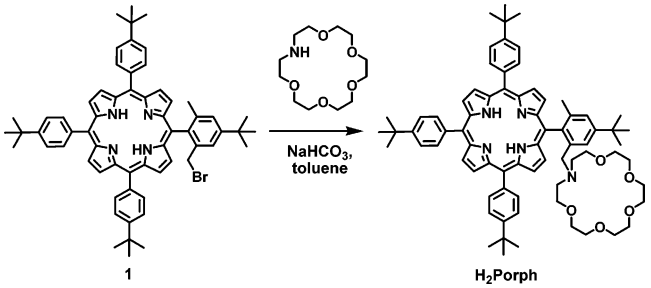

are high-spin species. The same authors studied the effect of electron-withdrawing groups on the stability and type of reactivity of the corresponding Fe(III)−peroxo complexes and showed that electron-withdrawing groups attached to the porphyrin macrocycle stabilize peroxo species and decrease nucleophilic reactivity.[10] Even the most stable Fe(III)−peroxo−porphyrin complex, $[Fe^{III}(F_{20}tpp)(O_2^{2-})]^-$, containing the very electron-poor $F_{20}tpp$ ligand ($F_{20}tpp$ = 5,10,15,20-tetrakis-(pentafluorophenyl)porphyrin), is stable only under an inert atmosphere for several weeks.[10] Interestingly, the same authors reported that addition of a potassium chelator to a solution of Fe(III)−peroxo species increases its stability,[9] suggesting the existence of an interaction between the potassium ion and the coordinated peroxo ligand.

It has been postulated, on the basis of the crystal structure of $[Mn^{III}(tpp)(O_2^{2-})]^-$, that the peroxide ligand in an Fe(III)−peroxo−porphyrin species is coordinated in a side-on bidentate manner.[12] However, it seems that the end-on form of these complexes leads to nucleophilic attack and that axial trans coordination of DMSO results in the opening of the triangular peroxo chelate ring, which increases the nucleophilicity of Fe(III)−peroxo species.[13a] Coordination of the axial ligand as a switch for chelate ring-opening of the peroxo ligand and a promoter of the nucleophilic reactivity was proposed to play a role in reactions of peroxo complexes derived from group VIII transition metals, as well as in enzymatic reactions.[13a] Interestingly, it has been demonstrated that side-on peroxo non-heme Fe(III) and Mn(III) species exhibit nucleophilic but not electrophilic reactivity.[13bc]

In this paper, we present the synthesis and characterization of the Fe(III) complex of a novel crown ether−porphyrin conjugate (H_2Porph) as ligand (Scheme 2, H_2Porph = 5^2-*N*-(4-aza-18-crown-6)methyl-5^4,10^4,15^4,20^4-tetra-*tert*-butyl-5^6-methyl-5,10,15,20-tetraphenylporphyrin)[14] and its reaction with KO_2. We also studied the kinetics and thermodynamics of the reaction of KO_2 and the Fe(II) form of the complex, which leads to a quite stable Fe(III)−peroxo−porphyrin species, $K[Fe^{III}(Porph)(O_2^{2-})]$. To our knowledge, kinetic and thermodynamic parameters for such reactions have not been previously reported. Even more interesting is the fact that the Fe(II) form of the studied complex can reversibly bind superoxide. The crown ether covalently attached to the porphyrin, as chelator of the electrophilic potassium cation, seems to play a role in the stabilization and reactivity of the peroxo complex studied. The release of O_2^- by the Fe(III)−peroxo species to form an Fe(II) species upon fine-tuning of the proton concentration is of biological interest, since this process might occur under physiological conditions.

Experimental Section

Materials. Reagents and solvents were obtained from commercial sources and were of reagent quality unless otherwise stated. DMSO and acetonitrile were purchased as extra-dry solvents. All chemicals were used as received without further purification. The preparation of the zinc complex of H_2Porph is described elsewhere.[14] The ligand H_2-ttbpp (5^4,10^4,15^4,20^4-tetra-*tert*-butyl-5,10,15,20-tetraphenylporphyrin) was obtained as a byproduct in the synthesis of a precursor of **1**. $K^{18}O_2$ was prepared according to the published method.[15] $^{18}O_2$ was obtained from Eurisotop, France. Fe(tpp) and Fe(oep) (tpp = *meso*-tetraphenylporphinato, oep = octaethylporphinato) were prepared according to an established literature method by metalation of the free ligands.[16] $^{57}FeCl_2$ was synthesized using ^{57}Fe powder (enrichment 95.95%, Medical Isotopes). $^{57}FeCl_2$ dihydrate was synthesized according to a literature method.[17] The light-blue dihydrate was dried in a drying pistol at 220 °C until a light brown color was obtained.

H_2Porph. The bromomethylporphyrin precursor **1**[18] (950 mg, 1 mmol), monoaza-18-crown-6 (290 mg, 1.1 mmol), and $NaHCO_3$ (92 mg, 1.1 mmol) were dissolved in dry toluene (25 mL) and refluxed for 24 h. The solvent was removed in vacuo, and the residue was purified by column chromatography (silica gel, eluent ethyl acetate/methanol 9:1). Yield: 914 mg (81% based on porphyrin precursor) of a dark violet product with metallic luster. ^{1}H NMR (400 MHz, $CDCl_3$, 25 °C): δ [ppm] = 8.91 (s, 4 H, β-pyrrole), 8.87 (d, 2 H, ^3J = 4.7 Hz, β-pyrrole), 8.67 (d, 2 H, ^3J = 4.7 Hz, β-pyrrole), 8.22 (d, 2 H, ^3J = 8.1 Hz, *o*-aryl-H), 8.17 (d, 4 H, ^3J = 7.7 Hz, *o*-aryl-H), 7.87 (d, 1 H, ^4J = 1.7 Hz, aryl-H), 7.79 (m, 6 H, *m*-Ar-H), 7.53 (d, 1 H, ^4J = 1.7 Hz, aryl-H), 3.19 (s, 2 H, aryl-methylene-H), 3.16 (m, 4 H, methylene-H), 3.14 (m, methylene-H), 2.98 (m, 4 H, methylene-H), 2.92 (m, 4 H, methylene-H), 2.69 (t, 4 H, ^3J = 6.1 Hz, methylene-H), 2.26 (t, 4 H, ^3J = 6.1 Hz, methylene-H), 1.97 (s, 3 H, methyl-H), 1.64 (s, 27 H, aryl-*tert*-butyl-H), 1.63 (s, 9 H, aryl-*tert*-butyl-H), −2.58 (s, 2 H, NH). ^{13}C NMR (100 MHz, $CDCl_3$, 25 °C): δ [ppm] = 150.9, 150.4 (3 C, *p*-aryl-C^q), ca. 147−145 (4 C, α-pyrrolic-C), 140.9, 139.3, 139.1, 138.9, 138.0, 134.5, ca. 131−130 (4 C, β-pyrrolic-C), 124.6, 123.6, 123.6, 123.12, 120.2, 119.8, 117.5, 70.2, 70.0, 69.7, 69.4, 59.1, 53.5, 34.9, 31.8, 31.7, 21.9. FAB-MS: *m*/*z* = 1129 (M^+), 865 (M^+ − monoaza-18-crown-6). UV/vis (CH_2Cl_2): λ_{max} [nm] (ϵ [L mol^{-1} cm^{-1}]) = 421 (335 000), 517 (13 500), 552 (6800), 590 (4100), 646 (4100). IR (KBr): $\tilde{\nu}$ [cm^{-1}] = 3316, 2957, 2902, 2865, 1474, 1362, 1350, 1108, 967, 801. Elemental analysis for $C_{74}H_{89}N_5O_5 \cdot 2H_2O$ calculated: C, 76.32; H, 8.05; N, 6.01. Found: C. 76.71; H, 7.72; N, 6.05.

[Fe^{III}(Porph)Cl]. H_2Porph (300 mg, 0.266 mmol) was dissolved in chloroform (30 mL). A solution of anhydrous $FeCl_2$ (50 mg, 0.391 mmol) in ethanol (30 mL) was added. Two drops of the base 2,6-

(6) Batinic-Haberle, I.; Spasojevic, I.; Hambright, P.; Benov, L.; Crumbliss, A. L.; Fridovich, I. *Inorg. Chem.* **1999**, *38*, 4011−4022.
(7) Kasugai, N.; Murase, T.; Ohse, T.; Nagaoka, S.; Kawakami, H.; Kubota, S. *J. Inorg. Biochem.* **2002**, *91*, 349−355.
(8) McCandlish, E.; Miksztal, A. R.; Nappa, M.; Sprenger, A. Q.; Valentine, J. S.; Stong, J. D.; Spiro, T. G. *J. Am. Chem. Soc.* **1980**, *102*, 4268−4271.
(9) Burstyn, J. N.; Roe, J. A.; Miksztal, A. R.; Shaevitz, B. A.; Lang, G.; Valentine, J. S. *J. Am. Chem. Soc.* **1988**, *110*, 1382−1388.
(10) Selke, M.; Sisemore, M. F.; Valentine, J. S. *J. Am. Chem. Soc.* **1996**, *118*, 2008−2012.
(11) Sisemore, M. F.; Selke, M.; Burstyn, J. N.; Valentine, J. S. *Inorg. Chem.* **1997**, *36*, 979−984.
(12) VanAtta, R. B.; Strouse, C. E.; Hanson, L. K.; Valentine, J. S. *J. Am. Chem. Soc.* **1987**, *109*, 1425−1434.
(13) (a) Selke, M.; Valentine, J. S. *J. Am. Chem. Soc.* **1998**, *120*, 2652−2653. (b) Park, M. J.; Lee, J.; Suh, Y.; Kim, J.; Nam, W. *J. Am. Chem. Soc.* **2006**, *128*, 2630−2634. (c) Seo, M. S.; Kim, J. Y.; Annaraj, J.; Kim, Y.; Lee, Y.-M.; Kim, S.-J.; Kim, J.; Nam, W. *Angew. Chem., Int. Ed.* **2007**, *46*, 377−380.
(14) Helmreich, M. Ph.D. thesis, University of Erlangen-Nürnberg, 2005.
(15) Rosenthal, I. *J. Labelled Compd. Radiopharm.* **1976**, *12*, 317−318.
(16) Borovkov, V. V.; Lintuluoto, J. M.; Inoue, Y. *Synlett* **1999**, 61−63.
(17) Janiak, C.; Dorn, T.; Paulsen, H.; Wrackmeyer, B. *Z. Anorg. Allg. Chem.* **2001**, *627*, 1663.
(18) Huyen, N. H.; Jannsen, U.; Mansour, H.; Jux, N. *J. Porphyrins Phthalocyanines* **2004**, *8*, 1356−1365.

lutidine were added, and the mixture was refluxed for 24 h open to the atmosphere. The reaction was monitored by thin-layer chromatography on alumina plates with CH_2Cl_2/methanol 9:1 as eluent. The reaction was completed when the typical fluorescence of the ligand had completely vanished. The reaction mixture was filtered to remove excess iron salts, and the solvent was evaporated. The product was purified by recrystallization from a mixture of pentane and dichloromethane to give a microcrystalline purple-black substance in 80% yield. ^{1}H NMR (400 MHz, $CDCl_3$, 25 °C): δ [ppm] = 84.8, 79.2, 77.9 (bs, 8 H, β-pyrrole), 17.9 (s, 1 H, *m*-aryl-H), 16.1 (s, 1 H, *m*-aryl-H), 13.9 (s, 3 H, *m*-aryl-H), 12.7 (s, 3 H, *m*-aryl-H), 2.61 (s, 36 H, aryl-*tert*-butyl-H). FAB-MS: m/z = 1217 (M^+), 1182 (M^+ − Cl). UV/vis (CH_2Cl_2): λ_{max} [nm] (ϵ [L mol^{-1} cm^{-1}]) = 384 (31 300), 420 (64 700), 512 (7740), 579 (2900), 701 (1860). IR (KBr): $\tilde{\nu}$ [cm^{-1}] = 3450, 2960, 2903, 2868, 1462, 1396, 1363, 1333, 1296, 1268, 1202, 1110, 1071, 999, 806, 723. Elemental analysis for $C_{74}H_{87}ClFeN_5O_5 \cdot 3H_2O$ calculated: C, 69.88; H, 7.37; N, 5.51. Found: C, 69.50; H, 7.56; N, 5.36.

[^{57}Fe^{III}(Porph)Cl]. The synthesis was carried out as for that of [Fe^{III}(Porph)Cl], except that anhydrous $^{57}FeCl_2$ was used instead of $FeCl_2$. The spectroscopic data (UV/vis, IR) were identical to those of the unlabeled compound.

[(Fe^{III}(Porph))$_2$O]. The bis-μ-oxo dimer was prepared by shaking a solution of [Fe^{III}(Porph)Cl] (50.0 mg, 0.041 mmol) in CH_2Cl_2 (20 mL) with a 2 M solution of aqueous NaOH (20 mL). The organic layer was separated and dried over anhydrous $MgSO_4$, and the solvent was evaporated. A brown solid was obtained in 94% yield. ^{1}H NMR (400 MHz, $CDCl_3$, 25 °C): δ [ppm] = 16.0, 14.3, 13.8, 12.6 (bs, 16 H, β-pyrrole), 8.30, 8.08, 7.78, 7.65, 7.53, 7.34, 7.32 (m, 28 H, *o*-aryl-H, *m*-aryl-H), 3.81, 3.74, 3.68, 3.63,3.61, 3.60, 3.55 (m, methylene-H of crown ether), 1.28 (s, 18 H, aryl-*tert*-butyl-H), 1.22 (s, 54 H, aryl-*tert*-butyl-H), 1.73−0.756 (m, aliphatic groups). ^{13}C NMR (100 MHz, $CDCl_3$, room temperature): δ [ppm] = 150.4, 123.3, 70.9, 70.8, 70.6, 70.4, 60.9, 52.8, 37.9, 34.4, 33.5, 31.8, 31.5, 29.4, 22.4. FAB-MS: m/z = 2380 (M^+). UV/vis (CH_2Cl_2): λ_{max} [nm] (ϵ [L mol^{-1} cm^{-1}]) = 414 (151 000), 514 (10 100), 574 (9930), 615 (5640). IR (KBr): $\tilde{\nu}$ [cm^{-1}] = 2961, 2925, 2866, 1731, 1461, 1394, 1362, 1335, 1262, 1201, 1110, 1026, 999, 863, 720.

K[Fe^{III}(Porph)(CN)$_2$]. [Fe^{III}(Porph)Cl] (50.0 mg, 0.041 mmol) was dissolved in CH_2Cl_2 (20 mL), and KCN (200 mg, 2.90 mmol) was added as a solid. The mixture was stirred for 24 h. The solution was filtered and the solvent evaporated. A green solid was obtained in 90% yield. ^{1}H NMR (400 MHz, $CDCl_3$, 25 °C): δ [ppm] = 9.78, 8.70, 8.53, 8.42 (8 H, *m*-aryl-H), 3.65, 3.64, 3.62, 3.61, 3.51, 3.40 (*m*-aryl-H, methylene-H), 3.19 (s, 2 H, aryl-methylene-H), 2.80 (s, 3 H, methyl-H), 2.49, 1.60 (methylene-H), 1.47, 1.35 (aryl-*tert*-butyl-H), 1.33, 1.25, 1.16, 1.14, 1.13 (methylene-H), −3.13, −3.32, −4.16, −4.39 (4s, 8 H, β-pyrrole). ^{13}C NMR (100 MHz, $CDCl_3$, room temperature): δ [ppm] = 156.6, 155.4, 150.6 (4 C, *p*-aryl-C^q), 127.8 (8 C, *o*-aryl-CH), 123.8 (8 C, *m*-aryl-CH), 85.4, 85.1, 84.0, 80.6 (8 C, β-pyrrole), 75.2, 75.1, 74.9, 73.3, 72.8, 70.9, 70.8, 70.7, 70.5 (OCH_2), 52.5 (aryl-CH_2), 33.6, 33.2 (8 C, *tert*-butyl-C^q), 32.0, 31.6 (24 C, *tert*-butyl-CH_3), 16.7 (6 C, CH_3). FAB-MS: m/z = 1272 (M^+). UV/vis (CH_2Cl_2): λ_{max} [nm] (ϵ [L mol^{-1} cm^{-1}]) = 333 (17 300), 433 (76 300), 539 (2530), 582 (2660), 678 (3110). IR (KBr): $\tilde{\nu}$ [cm^{-1}] = 2961, 2902, 2866, 2115, 1794, 1529, 1505, 1461, 1394, 1351, 1300, 1265, 1201, 1110, 1011, 951, 812, 792, 712.

[Fe^{III}(Porph)(DMSO)$_2$]$^+$. A solution of [Fe^{III}(Porph)Cl] in DMSO yielded the bis-solvent complex of the iron−porphyrin. ^{1}H NMR (300 MHz, DMSO-d_6, room temperature): δ [ppm] = 71.46, 70.74, 11.33, 9.67, 8.27, 7.52, 7.01, 5.08, 4.97, 4.24, 2.59, 2.49, 2.39, 2.06, 1.89, 1.57, 1.22, 1.13. UV/vis (DMSO): λ_{max} [nm] (ϵ [L mol^{-1} cm^{-1}]) = 399 sh (69 660), 420 (80 800), 531 (9870), 588 sh (1010), 650 (1850), 695 (2520).

[Fe^{III}(Porph)OH]. Addition of hydroxide ions as water or NaOH to a solution of [Fe^{III}Porph(DMSO)$_2$]$^+$ yielded the hydroxo complex [Fe^{III}(Porph)OH]. ^{1}H NMR (300 MHz, DMSO-d_6, room temperature): δ [ppm] = 80.46. UV/vis (DMSO): λ_{max} [nm] (ϵ [L mol^{-1} cm^{-1}]) = 423 sh (76 600), 429 (80 000), 518 (6670), 563 (4550), 583 (4180), 645 (2630), 710 (560).

[Fe^{II}(Porph)]. The reduced form of [Fe^{III}(Porph)Cl] could be obtained by chemical reduction or bulk electrolysis. Chemical reduction in dry DMSO was achieved by using sodium dithionite (saturated solution), potassium superoxide (KO_2, see below), cobaltocene, or nickelocene (1:5 Fe(III):reductant molar ratio) as reductant. In the case of superoxide, a 10^{-5} M solution of [Fe^{III}(Porph)Cl] in dry DMSO was prepared, and a solution containing a 10-fold excess of KO_2 in dry DMSO was added. UV/vis (DMSO): λ_{max} [nm] (ϵ [L mol^{-1} cm^{-1}]) = 412 sh (35 500), 430 (230 000), 531 (9670), 561 sh (5110), 585 sh (3550), 650 sh (2220), 700 sh (1400). ^{1}H NMR (reduction with cobaltocene, 300 MHz, DMSO-d_6, 25 °C): δ [ppm] = 10.37, 7.77, 7.53, 7.28, 6.51, 6.13, 6.036.19, 3.07, 2.96, 2.88, 2.25, 1.99, 1.70, 1.30.

K[Fe^{III}(Porph)(O$_2^{2-}$)]. KO_2 was suspended in a solution of [Fe^{III}(Porph)Cl] in dry DMSO. The solution was stirred until the color changed to green and was filtered under argon atmosphere. UV/vis (DMSO): λ_{max} [nm] (ϵ [L mol^{-1} cm^{-1}]) = 429 sh (39 500), 440 (197 000), 550 sh (8320), 570 (11 280), 597 sh (6230), 615 (5500), 628 (5120).

Equipment. Elemental analysis was performed on a HERAEUS CHN-Mikroautomat. A Hewlett-Packard 8452A spectrophotometer was used for UV/visible spectrophotometric measurements. NMR spectra in $CDCl_3$ and DMSO-d_6 were measured on a JEOL GX 400 NMR instrument or a Bruker Avance 300. All spectra were recorded using 5 mm o.d. NMR tubes, and chemical shifts were reported as δ (ppm) values calibrated to natural abundance deuterium solvent peaks (ppm). The IR spectra were recorded on a Mattson FT IR 60 AR instrument using liquid samples as films between KBr and NaCl plates, respectively. The spectrum of DMSO was used as reference. Porphyrin solutions were prepared by dissolving the solid sample in dry DMSO to give a 0.5 mM solution. The samples of the peroxo species were prepared by suspending solid KO_2 in the complex solution until the color change occurred, indicating formation of the peroxo species. After that, the mixture was filtered using a syringe filter, and the UV/vis spectrum was recorded to confirm the presence of the peroxo species. The neat KO_2 solutions were prepared by suspending solid KO_2 in dry DMSO and filtered through a syringe filter.

Cyclic voltammetric measurements were carried out using an Autolab instrument with a PGSTAT 30 potentiostat. A conventional three-electrode arrangement was employed, consisting of a gold working disc electrode (Metrohm, geometric area 0.07 cm^2), a platinum wire (Metrohm) as the auxiliary electrode, and Ag wire as a pseudo reference electrode. All measurements were done in DMSO in the presence of 0.1 M tetraethylammonium hexafluorophosphate as supporting electrolyte. The Fc^+/Fc (Fc = ferrocene) couple was used to calibrate the redox potentials, which are reported in volts vs SCE ($E_{1/2}$(Fc^+/Fc) = 0.43 V vs SCE).[19] All solutions without superoxide were thoroughly degassed with nitrogen prior to being used, and during the measurements a nitrogen atmosphere was maintained. Measurements with superoxide were carried out by saturating the solution with dry air. Sample concentration was 1.0 mM. All experiments were performed at room temperature.

Electrochemical reduction was performed under nitrogen at a Pt gauze working electrode with a Ag wire pseudo reference electrode and a Pt mesh auxiliary electrode, separated from the working electrode compartment by a glass frit. The electrolysis was terminated when the potential exceeded 0.5 V more negative than that of the Fe$^{III/II}$ couple.

Mössbauer Measurements. ^{57}Fe Mössbauer spectroscopy was done in frozen DMSO solution on a Mössbauer spectrometer operating in standard transmission geometry with an MR260A drive system and an MVT-1000 transducer (both from Wissenschaftliche Elektronik GmbH, Starnberg) with a 25 mCi ^{57}Co(Rh) source in symmetric triangle velocity

(19) Connelly, N. G.; Geiger, W. E. *Chem. Rev.* **1996**, *96*, 877−910.

mode. The temperature was controlled by a type ITC502 temperature controller (Oxford Instruments) inside a continuous-flow cryostat, type CF 506 (Oxford Instruments). Data were collected with a CMCA-550 data acquisition card (Wissenschaftliche Elektronik GmbH, Starnberg). Calibration was carried out by use of the inner four lines of the six-line pattern of α-iron at room temperature. Spectra were fitted by Lorentzians using the software "EFFI" (Hartmut Spiering, Mainz). The [$^{57}Fe^{III}$(Porph)Cl] complex (7.00 mg) was dissolved in dry DMSO (0.4 mL) under an atmosphere of argon in a drybox. To obtain the Fe(II) and Fe(III)−peroxo species, an excess of sodium dithionite or potassium superoxide, respectively, was added to the [$^{57}Fe^{III}$(Porph)Cl] solution and the resulting slurry was stirred for 15 min. This solution was filtered through a syringe filter, put into a Kel-F polychlorotrifluoroethylene (PCTFE) container, and sealed with a plug. The samples were immediately frozen in liquid nitrogen upon removal from the drybox.

Structural Determination of [Fe^{III}(Porph)Cl]·H_3O^+·$FeCl_4^-$·C_6H_6·EtOH. Purple needle-shaped crystals suitable for X-ray diffraction were obtained by slow diffusion of pentane into a benzene solution of the raw material obtained directly from the reaction mixture after its filtration and solvent evaporation. [Fe^{III}(Porph)Cl] cocrystallized with crown ether coordinated water, ethanol, benzene, and one unit of tetrachloroiron(III) acid. The ethanol molecule in the structure showed disorder due to an inversion center (50:50 occupation). An Enraf-Nonius KappaCCD area detector was used for data collection at 173 K. Cell parameters were obtained from 10 frames using a 10° scan and refined with 17 871 reflections. The structure was solved by using direct methods. The complex crystallizes in the space group $P\bar{1}$ with two formula units per unit cell. Calculations were carried out with the SHELX software,[20] and the graphics were generated with ORTEP-3.[21] Further details can be found in Table S2 in the Supporting Information.

Preparation of Superoxide Solution. The moisture-sensitive KO_2 solution was prepared and handled either under a nitrogen or an argon atmosphere by using standard Schlenck techniques or in an MBraun glovebox under an argon atmosphere. A slurry of KO_2 (200 mg, 2.82 mmol) in a 0.1 M solution of NBu_4PF_6 in DMSO (20 mL) was vigorously stirred for 30 min. The mixture was filtered through a syringe filter and the filtrate kept in the dark. Such a stock solution was stable (not more than 5% decrease in concentration) for about 5 h. Solutions of desired superoxide concentrations were prepared by diluting this stock solution with a DMSO solution of the electrolyte immediately before use, and the concentration was determined spectrophotometrically before and after measurement. Whenever the concentration of superoxide decreased during the course of an experiment by more than 5%, the results were discarded.

The superoxide solution in the DMSO/CH_3CN mixture was prepared according to the following procedure. Solid KO_2 (1 mg, 0.014 mmol) and *cis*-dicyclohexano-18-crown-6 (52.1 mg, 0.140 mmol) were weighed directly into the electrolyte solution (14 mL of 0.1 M $(NBu_4)PF_6$ in a 30:70 mixture of DMSO/CH_3CN) and stirred until completely dissolved. This solution was also kept in the dark; however, within approximately 30 min the concentration decreased by 5%.

Concentration of Superoxide Solution. The concentration of saturated KO_2 in 0.1 M NBu_4PF_6 in DMSO was determined to be 4.0 ± 0.1 mM by optical absorbance measurements (0.1 mm pathlength cell)[22] as well as by ferricytochrome *c* titration.[23] The same methods were used to determine the concentration of saturated KO_2 in DMSO without electrolyte, which was found to be 2.5 ± 0.2 mM.

Kinetic Measurements. Kinetic data were obtained by recording time-resolved UV/vis spectra using a modified μSFM-20 Bio-Logic stopped-flow module combined with a Huber CC90 cryostat and equipped with a J&M TIDAS high-speed diode array spectrometer with combined deuterium and tungsten lamps (200−1015 nm wavelength range). Isolast O-rings were used for all sealing purposes to enable measurements in DMSO, and solutions were delivered from 10 mL gastight Hamilton syringes. The syringes are controlled by separate drives, allowing for variation of the ratio of mixing volumes used in the kinetic runs. Data were analyzed by using the integrated Bio-Kine software, version 4.23, and also the Specfit/32 program. At least five kinetic runs were recorded under all conditions, and the reported rate constants represent the mean values. The stopped-flow instrument was thermostated to the desired temperature ±0.1 °C. Experiments at 25 °C were performed in DMSO solution, whereas for the low-temperature measurements a solution of 30% DMSO in CH_3CN was used. During all kinetic measurements, the ionic strength was kept constant at 0.1 M NBu_4PF_6. The reaction was followed in excess of KO_2, and the applied complex concentration was in the range of 5×10^{-5}−5×10^{-6} M. Concentration-dependent measurements were performed by mixing different concentrations of KO_2 with the same complex concentration in a 1:1 volume ratio and also by using the same KO_2 solution ([KO_2] = 2 and 0.2 mM, corresponding to 50% and 5% of the saturated KO_2 solution in DMSO, respectively) and applying the variable-mixing-volume-ratio option. For temperature dependence measurements in the DMSO/CH_3CN mixture within the −40 to 0 °C temperature range, a 1 mM solution of KO_2 was mixed with a 1×10^{-5} M solution of the complex in a 1:1 volume ratio. Because of the decreased stability of KO_2 in the DMSO/CH_3CN solvent mixture, a fresh KO_2 solution was prepared every 0.5 h, so that the concentration decrease was not greater than 5%. Values of $\Delta H^{\ddagger}$ and $\Delta S^{\ddagger}$ were calculated from the slope and intercept, respectively, of the plot of $\ln(k/T)$ versus $1/T$ (the second-order rate constant k was defined as $k_{obs}/[O_2^-]$).

Equilibrium Measurement. A spectrophotometric study of the binding of superoxide to [Fe^{II}(Porph)$(DMSO)_2$] was performed in a 1 cm path length cuvette with a 25 mL reservoir under nitrogen. The 5×10^{-6} M solution (20 mL) of [Fe^{II}(Porph)$(DMSO)_2$] complex in 0.1 M NBu_4PF_6 was purged with dry nitrogen for 20 min, and then aliquots of spectrophotometrically verified saturated KO_2 solution were added from a Hamilton microsyringe. The titration spectra were analyzed with Specfit/32 using the M/L/H^+ model, treating all components as colored species, and taking into consideration the dilution effects. The same procedure was repeated by using a 1×10^{-5} M solution of [Fe^{II}(Porph)$(DMSO)_2$] and DMSO−KO_2 solutions without electrolyte.

Results and Discussion

Synthesis and Structure. The novel porphyrin−crown ether conjugate H_2Porph used in this work[14] is a tetraphenylporphyrin with *tert*-butyl groups at the para position of the porphyrin which enhance the solubility in organic solvents. H_2Porph is easily accessible via a nucleophilic substitution reaction of the bromomethylated porphyrin precursor **1**[18] (Scheme 2) in the presence of sodium bicarbonate as acid scavenger. Aza-18-crown-6 is attached through its amine group to a methyl group at the ortho position of one aryl ring. This close proximity of the crown ether gives the metalated form of the ligand its unique properties. The metalloporphyrin can function as a ditopic receptor by coordinating a potassium cation, which can then interact with a diatomic anionic ligand bound to the metal center. Such an interaction has already been confirmed by X-ray structure analysis of the corresponding zinc(II) and cobalt(III) complexes with one and two coordinated cyanide anions, respectively.[14] In both cases, a potassium ion is coordinated in the crown ether, which is positioned directly over the porphyrin ring. A similar behavior is expected for the analogous iron(III)−porphyrin complex reported herein.

(20) Sheldrick, G. M. *SHELXS-97 and SHELXL-97*, programs for crystal structure solution and structure refinement; Universität Göttingen: Göttingen Germany, 1997.
(21) ORTEP-3 for Windows 1.06: Farrugia, L. J. *J. Appl. Crystallogr.* **1997**, *30*, 565.
(22) Sawyer, D. T.; Calderwood, T. S.; Yamaguchi, K.; Angelis, C. T. *Inorg. Chem.* **1983**, *22*, 2577−2583 and references therein.
(23) Arudi, R. L.; Allen, A. O.; Bielski, B. H. J. *FEBS Lett.* **1981**, *135*, 265−267.

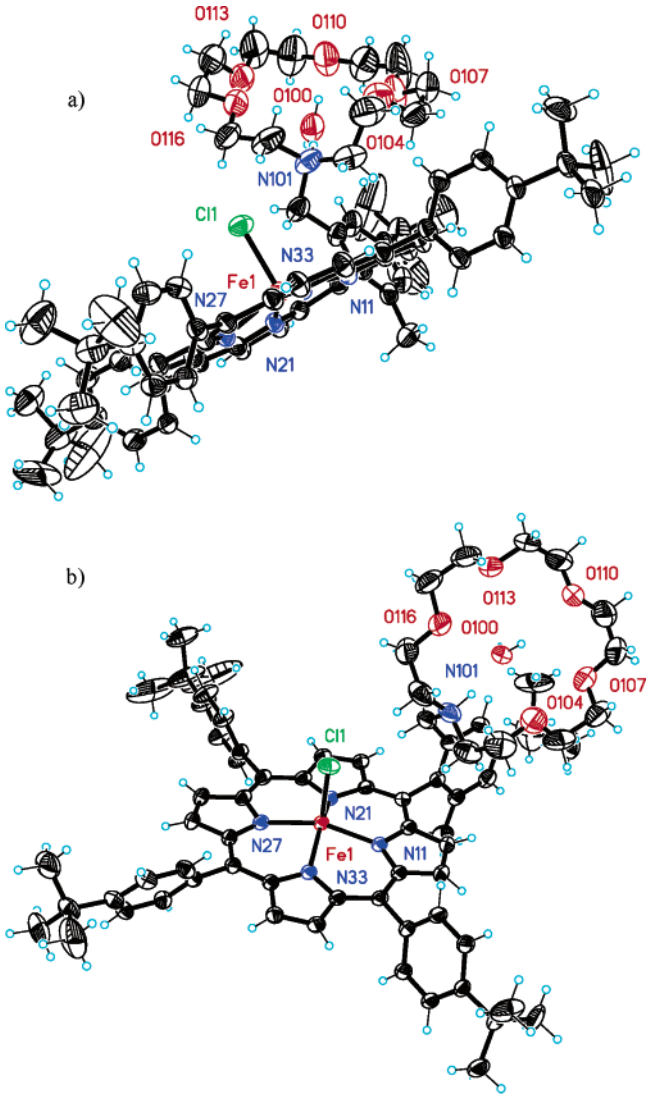

Figure 1. ORTEP representation of $[Fe^{III}(Porph)Cl]\cdot H_3O^+$: (a) side view and (b) top view.

The metalloporphyrin $[Fe^{III}(Porph)Cl]$ was prepared according to an established procedure[16] by refluxing a chloroform solution of the ligand with an ethanolic solution of ferrous chloride in the presence of 2,6-lutidine. When the material was crystallized from dichloromethane/pentane mixtures, analytically pure high-spin chloro iron(III)−porphyrin was obtained. The resonances of the β-pyrrolic protons of the porphyrin were found in the typical region of around 77−80 ppm. If pentane was allowed to diffuse slowly into a solution of freshly prepared material in benzene, crystals suitable for X-ray structural analysis grew. Interestingly, $[Fe^{III}(Porph)Cl]$ cocrystallized with a crown-ether-coordinated water molecule and one unit of tetrachloroiron(III) acid, its proton most likely bound to the nitrogen atom of the crown ether (Figure 1). Also, one molecule each of ethanol and benzene are found in the lattice. Although structural resolution was not formidable (R factor = 7.5%), the data obtained show a typical high-spin five-coordinate Fe(III) center with the chloro ligand pointing to the coordinated water molecule in the crown ether. The metal center is displaced by 0.47 Å from the mean porphyrin plane toward the crown ether. A water molecule bound within the crown ether interacts with the protonated nitrogen atom of the crown ether. The overall topology is most probably engendered by electrostatic interaction between the anionic chloro ligand and the cationic crown ether (the Cl1−N101 distance is 4.44 Å). Further structural data are given as Supporting Information (Tables S2 and S3).

The bis(cyano)iron(III) complex of H_2Porph was also synthesized to study the influence of the potassium ion on the spin state of the iron center. Synthesis was performed by stirring solid KCN with $[Fe^{III}(Porph)Cl]$ in dichloromethane, which takes up the KCN—most likely with the crown ether acting as a phase-transfer catalyst. The bis(cyano) complex $K[Fe^{III}Porph(CN)_2]$ was first examined by proton NMR spectroscopy. The spectrum shows an iron(III)−porphyrin low-spin complex ($S = {}^1/_2$) with four resonances for the pyrrolic protons between −3 and −5 ppm. This high-field shift is not very strong relative to those of similar low-spin iron(III)−porphyrins[24] that have pyrrole proton resonances around −16 ppm. Thus, the complex exists in the $(d_{xz},d_{yz})^4(d_{xy})^1$ spin state rather than the more usual $(d_{xy})^2(d_{xz},d_{yz})^3$ spin state. The $(d_{xz},d_{yz})^4(d_{xy})^1$ spin state is known[25] to occur in the presence of solvents that can form hydrogen bonds to the cyanide ligands, thus increasing their π-acceptor ability, which leads to back-bonding from the iron center to the cyanide ligands and not to the porphyrin ring. In our case, this effect is too strong to be caused by the deuterochloroform solvent, which can only form weak hydrogen bonds to the cyanide ligands. Our conclusion is that this strong increase in π-acceptor ability at the cyanide ligands can only come from interaction with the positively charged potassium ion coordinated by the crown ether, which pulls electron density away from the ligands. This was confirmed by a proton NMR experiment with $Bu_4N^+CN^-$ instead of KCN. $Bu_4N^+CN^-$ was mixed with $[Fe^{III}(Porph)Cl]$ in $CDCl_3$ in the NMR tube, and the spectrum was recorded. In this case, the shift to higher field by the pyrrolic protons is stronger (−8 to −10 ppm) than that observed with our bis(cyano) complex. We interpret this to mean that the bulky Bu_4N^+ cation cannot be coordinated by the crown ether, and, therefore, only interaction between solvent and cyanide occurs. These results show that our iron(III)−porphyrin acts as a ditopic receptor for diatomic anions as it has been demonstrated in the crystal structures of the corresponding zinc and cobalt complexes.[14] A strong electrostatic interaction, like the one between chelated K^+ and CN^-, is also to be expected between chelated K^+ and the peroxide anion (see below) and may be one of the reasons for the enhanced stability of the peroxo species.

We also performed proton NMR experiments in DMSO-d_6 on $[Fe^{III}(Porph)Cl]$ because our further experiments were carried out in this solvent. $[Fe^{III}(Porph)Cl]$ shows the behavior typical of an iron(III)−porphyrin in DMSO, having lost the chloro ligand and coordinated two DMSO molecules upon solvation.[26,27] This can be observed by the shift of the resonances of the pyrrolic protons from around 82 ppm in $CDCl_3$ to around 72 ppm in DMSO.[27,28] Trace amounts of the hydroxo complex were also observed in the NMR spectrum of the Fe(III) complex, with a broad resonance at 80 ppm.

UV/Vis Spectra. The property of the $[Fe^{III}(Porph)Cl]$ complex to act as a ditopic receptor toward diatomic anions is very attractive for studying its reaction with superoxide. The reaction

(24) La Mar, G. N.; Walker, F. A. *J. Am. Chem. Soc.* **1973**, *95*, 1782−1790.
(25) Ikezaki, A.; Nakamura, M. *Inorg. Chem.* **2002**, *41*, 2761.
(26) Kadish, K. M.; Bottomley, L. A.; Beroiz, D. *Inorg. Chem.* **1978**, *17*, 1124.
(27) Shin, K.; Kramer, S. K.; Goff, H. M. *Inorg. Chem.* **1987**, *26*, 4103−4106.
(28) Zobrist, M.; La Mar, G. N. *J. Am. Chem. Soc.* **1978**, *9*, 61−79.

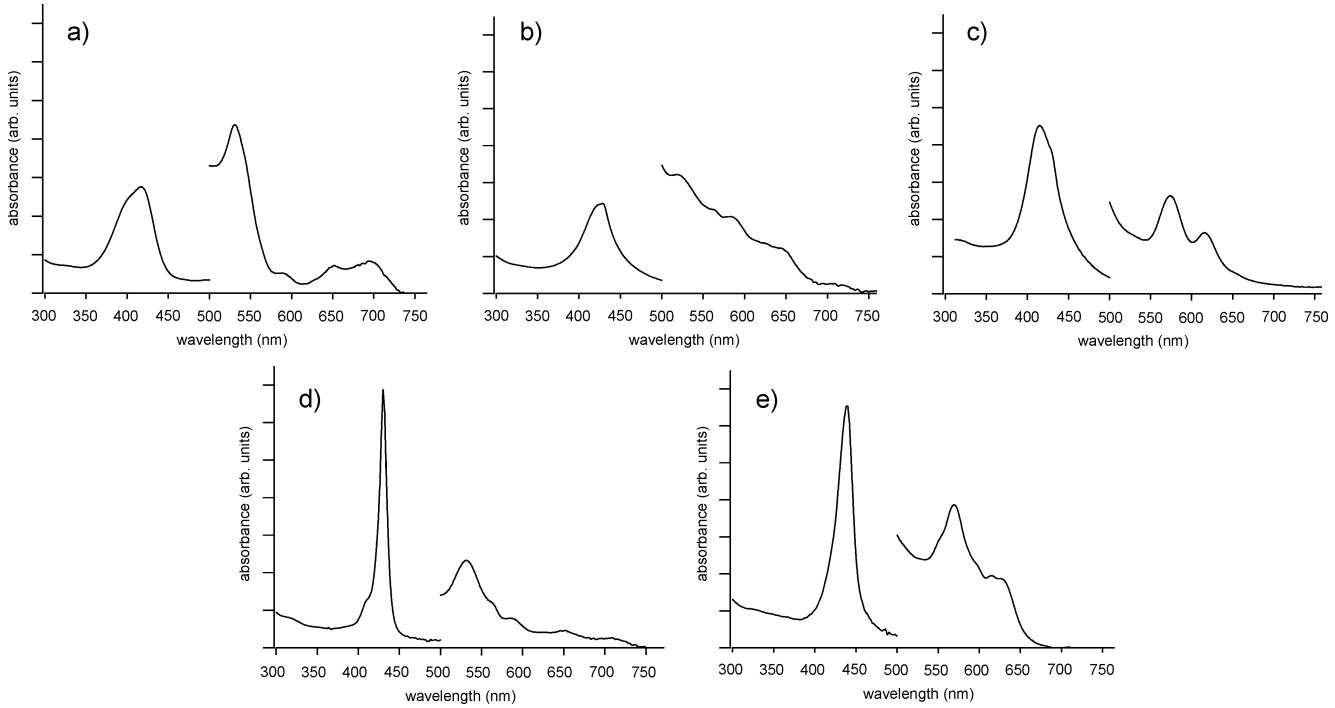

Figure 2. UV/vis absorption spectra of (a) $[Fe^{III}Porph(DMSO)_2]^+$, (b) $[Fe^{III}(Porph)OH]$, (c) $[(Fe^{III}(Porph))_2O]$, (d) $[Fe^{II}(Porph)(DMSO)_2]$, and (e) $K[Fe^{III}(Porph)(O_2^{2-})]$.

of Fe(III)−porphyrins with superoxide is convenient to follow in DMSO as aprotic solvent, in which the solubility and stability of KO_2 (a common source of O_2^-) are satisfactory. It is also known that the use of potassium chelators will enhance the solubility of KO_2. Moreover, the presence of potassium chelators can influence the properties of the product species that result from the reaction between Fe(III)−porphyrin complexes and superoxide.[9]

Dissolution of $[Fe^{III}(Porph)Cl]$ in DMSO produces an $[Fe^{III}(Porph)(DMSO)_2]^+$ complex with a characteristic Soret band at 420 nm and a shoulder at 399 nm (Figure 2a). In wet DMSO or upon addition of NaOH, a hydroxo complex is formed with a Soret band at 429 nm (Figure 2b); a dimer does not form in DMSO. The UV/vis spectrum of separately synthesized $[(Fe^{III}(Porph))_2O]$ (see the Experimental Section) in DMSO shows a Soret band at 414 nm with a shoulder at 429 nm (Figure 2c). By adding acid (trifluoromethanesulfonic acid, HOTf) to the solution of the hydroxo or dimer species, the spectrum of $[Fe^{III}(Porph)(DMSO)_2]^+$ was obtained.

The reaction of $[Fe^{III}(Porph)(DMSO)_2]^+$ and KO_2 was investigated using a tandem cuvette. When a 10-fold excess of superoxide is mixed with the $[Fe^{III}(Porph)(DMSO)_2]^+$ complex, reduction of the Fe(III) center is observed, as indicated by the shift of the Soret band maximum from 420 to 430 nm[8] (step I in Scheme 3). Reduction of the iron center by superoxide is confirmed by comparison of the resulting spectrum (Figure 2d) to the one obtained by electrochemical (see Experimental Section) or chemical (by sodium dithionite) reduction of $[Fe^{III}(Porph)(DMSO)_2]^+$ (Figure 3). When a larger excess of superoxide (≥20-fold) is added to the solution of $[Fe^{III}(Porph)(DMSO)_2]^+$, a peroxo complex, $[Fe^{III}(Porph)(O_2^{2-})]^-$, is formed (step II in Scheme 3), accompanied by a shift in the Soret band maximum to 440 nm. The spectrum of the obtained peroxo species (Figure 2e) is strikingly similar to the visible absorption

Scheme 3

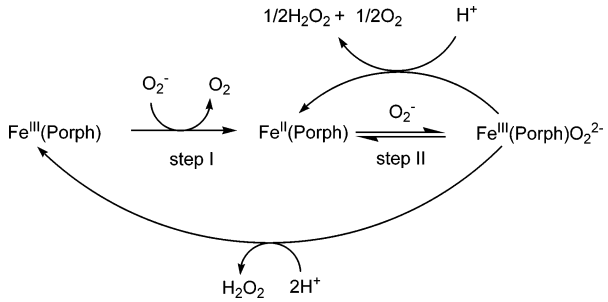

spectrum of the peroxo $[Fe^{III}(tpp)O_2^{2-}]^-$ complex obtained in the presence of a potassium chelating agent.[29] The low-energy Soret band (440 nm) and the splitting of the two Q bands are characteristic for an iron(III)−porphyrin with a peroxo ligand.[8]

Reversible Binding of Superoxide. In the presence of excess superoxide in the solution, the green $[Fe^{III}(Porph)(O_2^{2-})]^-$ complex (λ_{max} = 440 nm) is quite stable, and there is no need to handle it under an inert atmosphere. The peroxo complex is indefinitely stable in a frozen DMSO solution, even upon exposure to air. In a closed system under air, it is stable at room temperature for a week. When the solution is opened to the atmosphere, slow transformation (within a few hours) to the $[Fe^{II}(Porph)]$ species is observed, as monitored by UV/vis spectroscopy. This reaction was found to be caused by absorption of moisture from the atmosphere, as no spectral changes are observed when the peroxo complex is purged with dry oxygen. The rate of decay of $[Fe^{III}(Porph)(O_2^{2-})]^-$ is accelerated by passing wet air through the solution, which results in the formation of the brown $[Fe^{II}(Porph)]$ complex, as monitored by UV/vis spectroscopy. Further addition of superoxide to the brown $[Fe^{II}(Porph)]$ complex results in re-formation of the green peroxo complex. Dilution of a solution of the peroxo complex

(29) See Figure 1 (top spectrum) in ref 8 and Figure 6B in ref 9.

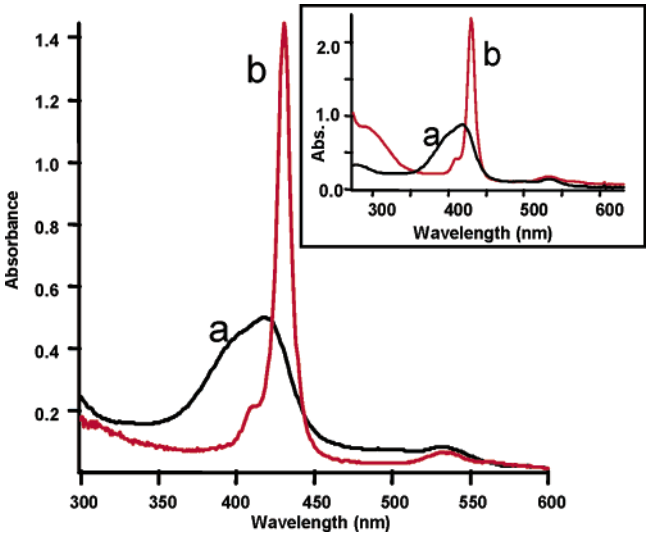

Figure 3. UV/vis spectra recorded in a tandem cuvette of the solution of 5×10^{-6} M $[Fe^{III}Porph(DMSO)_2]^+$ and 5×10^{-5} M KO_2 in DMSO at room temperature, (a) before ($\lambda_{max} = 420$ nm) and (b) after ($\lambda_{max} = 430$ nm) mixing. Inset: UV/vis spectra of 5×10^{-6} M $[Fe^{III}Porph(DMSO)_2]^+$, (a) before ($\lambda_{max} = 420$ nm) and (b) after ($\lambda_{max} = 430$ nm) reduction by dithionite.

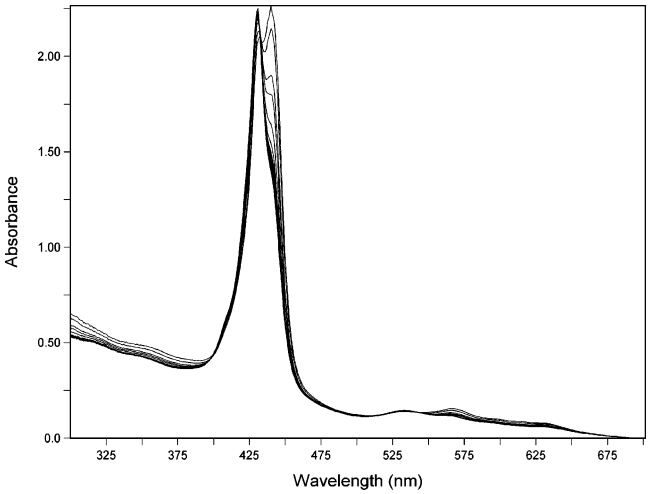

Figure 4. Time-resolved spectra for the reaction of $K[Fe^{III}(Porph)(O_2^{2-})]$ and HOTf at 25 °C in DMSO; $[K[Fe^{III}(Porph)(O_2^{2-})]] = 1 \times 10^{-5}$ M, $[HOTf] = 5 \times 10^{-5}$ M.

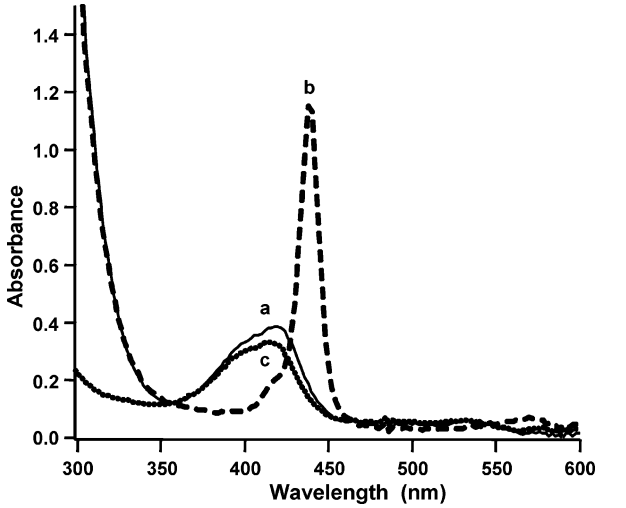

Figure 5. UV/visible absorption spectra of (a) $[Fe^{III}(Porph)(DMSO)_2]^+$, (b) $K[Fe^{III}(Porph)(O_2^{2-})]$, and (c) $K[Fe^{III}(Porph)(O_2^{2-})]$ + 0.1 M HOTf.

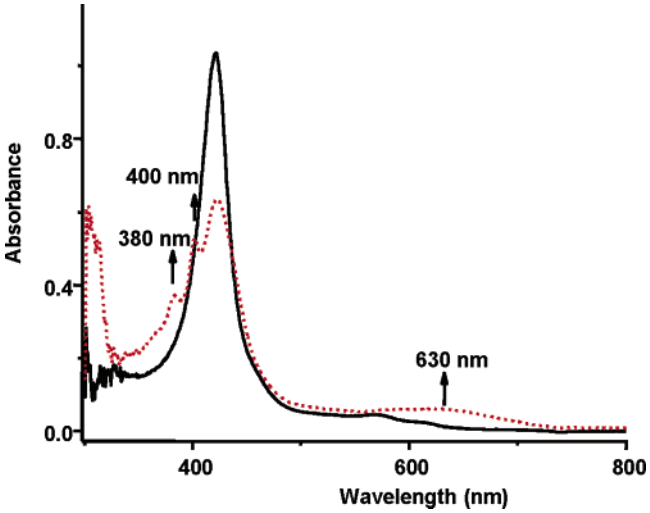

Figure 6. Spectral changes upon mixing 10^{-3} M MCPBA with a solution of 10^{-1} M TBPH and 1.3×10^{-5} M $[Fe^{III}(Porph)Cl]$ in KCl-saturated $DMSO/CH_3CN$ (5% DMSO) solution at room temperature, before (black solid line) and after mixing (red dotted line).

results in partial formation of the $[Fe^{II}(Porph)]$ complex, whereas further addition of superoxide to the diluted solution again restores the peroxo complex. All these observations suggest that the binding of superoxide to the Fe(II) complex is reversible and that the decrease in concentration of O_2^-, caused by its decomposition in the presence of protons, shifts the equilibrium from the Fe(III)−peroxo to the Fe(II) complex. Addition of a moderate excess of triflic acid to the peroxo complex causes partial formation of the $[Fe^{II}(Porph)]$ complex (Figure 4) by facilitating the decay of superoxide in the solution. When a large excess of acid is added, the $[Fe^{III}(Porph)(DMSO)_2]^+$ complex is formed (Figure 5). Scheme 3 summarizes the observed reactions.

To test for the presence of a high-valent iron−oxo species as a decay product of the peroxo complex, the trap 2,4,6-tri-(*tert*-butyl)phenol (TBPH) was utilized. Typically, upon oxidation, TBPH forms an oxygen-centered radical, which results in an increase of absorbance at 380, 400, and 630 nm.[30] In a separate experiment, we generated an iron−oxo species in the presence of K^+ (KCl), DMSO (30% DMSO in CH_3CN), and TBPH by using *m*-chloroperbenzoic acid (MCPBA) (Figure S1, Supporting Information).[30] As expected, formation of the high-valent iron−oxo species in the solution caused increases in the absorbance at 380, 400, and 630 nm (Figure 6). As MCPBA is not very stable in DMSO, decreasing the amount of DMSO in solution resulted in even more pronounced spectral changes (Figure 6). However, upon addition of TBPH to the solution of $[Fe^{III}(Porph)(O_2^{2-})]^-$, no evidence for a high-valent iron−oxo species was observed, but $[Fe^{II}(Porph)]$ was produced instead (Figure S2, Supporting Information). (The same was observed when triflic acid and an excess of TBPH were added to the solution of $[Fe^{III}(Porph)(O_2^{2-})]^-$.) In a subsequent study, TBPH was also found to react with superoxide; comparison of the spectral changes with those upon reaction with NaOH indicates that TBPH is acting as an acid. Phenols are known to act as

(30) (a) Traylor, T. G.; Lee, W. A.; Stynes, D. V. *J. Am. Chem. Soc.* **1984**, *106*, 755−764. (b) Traylor, T. G.; Lee, W. A.; Stynes, D. V. *Tetrahedron* **1984**, *40*, 553−568.

Scheme 4

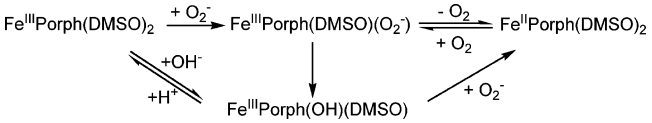

moderate acids to protonate superoxide ion in aprotic solvents and induce its efficient disproportionation ($K = 10^{18}$).[31] The protonation of superoxide present in an equilibrium solution causes its decay,[31,32] shifting the equilibrium from [Fe^{III}(Porph)-(O_2^{2-})]$^-$ to [Fe^{II}(Porph)] (Scheme 3, Figure S2). This process has been exploited in the kinetic studies of the unique reversible binding of superoxide for direct determination of the rate constant for dissociation of superoxide (back reaction of step II in Scheme 3).

The reaction between [Fe^{II}(Porph)] and O_2 (the reverse of the reaction between [Fe^{III}(Porph)($DMSO)_2$]$^+$ and O_2^-) was investigated to check the reversibility of the first step in Scheme 3. [Fe^{II}(Porph)] (2.5×10^{-6} M), prepared by electrochemical reduction of [Fe^{III}(Porph)($DMSO)_2$]$^+$, and O_2-saturated DMSO (1 atm, [O_2] = 2.2 mM)[21] were mixed in equal proportions in an Ar-flushed tandem cuvette. The resulting product (Figures S3 and S4, Supporting Information) was found to be not [Fe^{III}-(Porph)($DMSO)_2$]$^+$ but rather the hydroxo species, as indicated by the absence of a Q-band at 530 nm, which is observed for both [Fe^{III}(Porph)($DMSO)_2$]$^+$ and [Fe^{II}(Porph)]. There is also the possibility that an O-bound adduct is formed, as the spectra of [Fe^{III}(Porph)(O_2^-)] and [Fe^{III}(Porph)OH] are expected to be similar, since both involve a negatively charged O ligand. A similar spectrum was observed for an intermediate or side product in the reaction of [Fe^{III}(Porph)($DMSO)_2$]$^+$ with KO_2 (Figure S4), which we have shown to be the spectrum of the hydroxo complex [Fe^{III}(Porph)OH] (see below). The reaction of [Fe^{II}(Porph)] and O_2 did not follow a single-exponential decay. It is possible that an [Fe^{II}(Porph)O_2] adduct is produced, which may decay further to the hydroxo complex.[33] When a solution of [Fe^{II}(Porph)] was purged at first with dried air (until the band at 430 nm decreased in intensity and broadened) and then with Ar, the spectrum of [Fe^{II}(Porph)] was recovered. Upon subsequent bubbling of air for a longer period, the 430 nm peak was observed to decrease further in intensity and increase again upon bubbling with Ar. Recovery of the spectrum of [Fe^{II}-(Porph)] was not complete in this case, which we attribute to formation of the hydroxo complex. Scheme 4 summarizes the observed reactions (see also Kinetics and Thermodynamics, below).

Electrochemistry. To examine the electrochemical properties of [Fe^{III}(Porph)Cl] and its reaction product with superoxide, cyclic voltammetric experiments were carried out in nitrogen- and oxygen-saturated DMSO solutions, respectively. By way of comparison, the cyclic voltammograms of the corresponding Zn(II) complex [Zn^{II}(Porph)] were measured in order to check the electrochemical behavior of the porphyrin ring itself, as zinc-(II) is electrochemically inactive. In general, the redox behavior of [Fe^{III}(Porph)Cl] and [Zn^{II}(Porph)] is in accordance with the redox behavior of [Fe^{III}(tpp)]$^+$ and [Zn^{II}(tpp)], respectively.[34] The results of the electrochemical studies are summarized in Scheme S1 and Figure S5 (Supporting Information).

Table 1. Mössbauer Parameters of the Studied Complexes in Frozen DMSO at 80 K

compound	δ (mm s^{-1})	ΔE_Q (mm s^{-1})	Γ_{li} (mm s^{-1})	Γ_{re} (mm s^{-1})
[Fe^{III}(Porph)($DMSO)_2$]Cl	0.375	0.829	0.863	1.516
[Fe^{II}(Porph)($DMSO)_2$]	0.442	1.314	0.274	0.249
[Fe^{II}(Porph)(DMSO)]	1.270	3.114	0.534	0.463
K[Fe^{III}(Porph)(O_2^{2-})][a]	0.407	0.512	0.319	0.322

[a] A low-spin Fe(II) species present in the same solution (see text) has δ = 0.358 mm s^{-1}, ΔE_Q = 1.377 mm s^{-1}, Γ_{li} = 0.034 mm s^{-1}, and Γ_{re} = 0.369 mm s^{-1}.

The redox potentials corresponding to the Fe(III)/Fe(II) couples of our complex are more positive than those of [Fe^{III}-(tpp)]$^+$,[34] suggesting higher stability of the complex in the Fe-(II) oxidation state. This was observed when [Fe^{II}(Porph)] was chemically or electrochemically generated, since it is stable under air for a few hours, whereas [Fe^{II}(tpp)] oxidizes immediately under air. The significant stability of [Fe^{II}(Porph)] enabled further kinetic and thermodynamic investigations.

Mössbauer Spectra. Mössbauer spectra of the ^{57}Fe-enriched [Fe^{III}(Porph)Cl], [Fe^{II}(Porph)], and K[Fe^{III}(Porph)(O_2^{2-})] species in DMSO solution were measured at 80 K. The Mössbauer spectrum of the starting complex, [Fe^{III}(Porph)($DMSO)_2$]$^+$ (obtained by dissolving ^{57}Fe-enriched [Fe^{III}(Porph)Cl] in DMSO), exhibits an isomer shift (δ) of 0.38 mm s^{-1} and a quadrupole splitting (ΔE_q) of 0.83 mm s^{-1} (Table 1), which are characteristic of high-spin porphyrinatoiron(III) complexes.[35] The Mössbauer spectrum of the chemically reduced (with sodium dithionite and also with cobaltocene), ^{57}Fe-enriched [Fe^{III}-(Porph)]$^+$ complex (Figure 7a) shows that there are two different iron(II) species in solution, a low-spin (δ = 0.44 mm s^{-1}, ΔE_q = 1.32 mm s^{-1}) and a high-spin (δ = 1.27 mm s^{-1}, ΔE_q = 3.11 mm s^{-1}) species (Table 1). Most probably, the low-spin species is the six-coordinate bis-DMSO [Fe^{II}(Porph)($DMSO)_2$] complex and the corresponding high-spin species is the five-coordinate mono-DMSO [Fe^{II}(Porph)(DMSO)] complex.[35a,36,37]

To obtain the Mössbauer spectrum of [Fe^{III}(Porph)(O_2^{2-})]$^-$, the ^{57}Fe-enriched [Fe^{III}(Porph)]$^+$ complex was treated with a large excess of KO_2 in DMSO. The spectrum (Figure 7b) shows the presence of both low-spin iron(II) species (δ = 0.36 mm s^{-1}, ΔE_q = 1.38 mm s^{-1}) and high-spin [Fe^{III}(Porph)(O_2^{2-})]$^-$ (δ = 0.41 mm s^{-1}, ΔE_q = 0.51 mm s^{-1}) (Table 1) and suggests an equilibrium between these two iron species and the reversible nature of superoxide binding. The Mössbauer parameters of the iron(II) species are typical for low-spin Fe(II) in hexacoordinate porphyrin complexes[36] and are in good agreement with those of the low-spin iron(II) species obtained by chemical (by sodium

(31) Chin, D.-H.; Chiericato, G., Jr.; Nanni, E. J., Jr.; Sawyer, D. T. *J. Am. Chem. Soc.* **1982**, *104*, 1296−1299.
(32) The products of superoxide disproportionation, O_2 and H_2O_2, were qualitatively detected in both experiments with triflic acid and TBPH. For the O_2 detection, see: Karlin, K. D.; Cruse, R. W.; Gultneh, Y.; Farooq, A.; Hayes, J. C.; Zubieta, J. *J. Am. Chem. Soc.* **1987**, *109*, 2668−2679. For the H_2O_2 detection, a peroxide indicator paper suitable for the organic solvents (QUANTOFIX-Peroxide 100) was used.
(33) Ghiladi, R. A.; Kretzer, R. M.; Guzei, I.; Rheingold, A. L.; Neuhold, Y.-M.; Hatwell, K. R.; Zuberbühler, A. D.; Karlin, K. D. *Inorg. Chem.* **2001**, *40*, 5754−5767.
(34) Jones, S. E.; Srivatsa, G. S.; Sawyer, D. T. *Inorg. Chem.* **1983**, *22*, 3903−3910.
(35) (a) Sams, J. R.; Tsin, T. B. Mössbauer Spectroscopy of Iron Porphyrins. In *The porphyrins*; Dolphin, D., Ed.; Academic Press: New York, 1979; Vol. 4, pp 425−478. (b) Abu-Soud, H.; Silver, J. *Inorg. Chim. Acta* **1988**, *52*, 61−66.
(36) Abu-Soud, H. M.; Silver, J. *Inorg. Chim. Acta* **1989**, *161*, 139−141.
(37) Andersson, L. A.; Mylrajan, M.; Loehr, T. M.; Sullivan, E. P.; Strauss, S. H. *New J. Chem.* **1992**, *16*, 569−576.

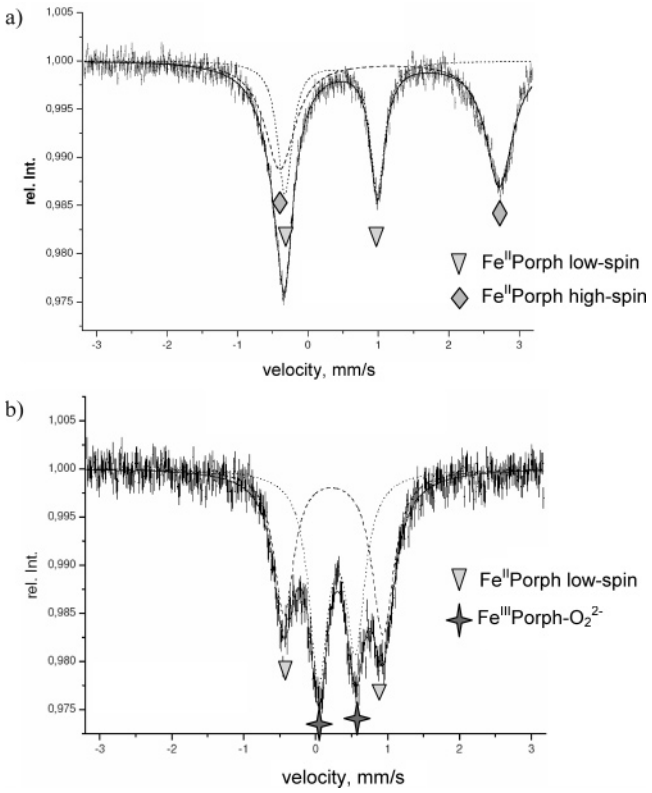

Figure 7. Mössbauer spectra of reduced ^{57}Fe-enriched [Fe^{III}(Porph)Cl] (a) and K[Fe^{III}(Porph)(O_2^{2-})] (b) complexes in frozen DMSO at 80 K.

dithionite and cobaltocene) reduction of the starting iron(III) complex (Table 1). The absence of the high-spin five-coordinate iron(II) species in the superoxide-saturated DMSO solution can be easily understood in terms of its higher reactivity and the presence of a vacant coordination site, resulting in its efficient trapping by superoxide and DMSO. This also suggests that the dissociation of DMSO from low-spin [Fe^{II}(Porph)($DMSO)_2$] and formation of high-spin five-coordinate [Fe^{II}(Porph)(DMSO)] as a reactive intermediate is the slowest reaction step in the formation of the Fe(III)−peroxo complex (see below).

The Mössbauer parameters of our iron(III)−peroxo complex are interesting. Although they are typical for high-spin iron(III)−porphyrin complexes, they are lower than those of known iron(III)−peroxo complexes.[35,38−40] Non-heme iron(III)−peroxo complexes, all of which are considered to be side-on η^2-O_2 peroxo species, have a characteristic large isomer shift located in the 0.62−0.65 mm s^{-1} range and a large quadrupole splitting in the 0.72−1.37 mm s^{-1} range.[38] The isomer shift of one of the first such species in a biological system for which Mössbauer parameters are available, the seven-coordinate side-on iron(III)−peroxo species of superoxide reductase, is slightly lower (δ = 0.54 mm s^{-1}), which was explained by the presence of the coordinated thiolate ligand.[39] Another example of an iron(III)−peroxo species with an isomer shift below the characteristic range is a μ-η^2:η^1 peroxo-bridged heme−copper complex (δ = 0.56 mm s^{-1}), with the quadrupole splitting in the expected range (ΔE_q = 1.17 mm s^{-1}).[40] The iron(III)−peroxo species with the Mössbauer parameters most similar to those of our [Fe^{III}(Porph)(O_2^{2-})]$^-$ is the [Fe^{III}(oep)(O_2^{2-})]$^-$ complex.[9] However, its isomer shift (δ = 0.67 mm s^{-1}) and quadrupole splitting (ΔE_q = 0.62 mm s^{-1}) are larger than in our case (Table 1). It should be mentioned that the Mössbauer measurements of [Fe^{III}(oep)(O_2^{2-})]$^-$ were performed on solid samples, whereas our measurements were performed on solutions in DMSO. This could have an influence on the type of interactions the peroxo ligand undergoes and consequently on its coordination mode.

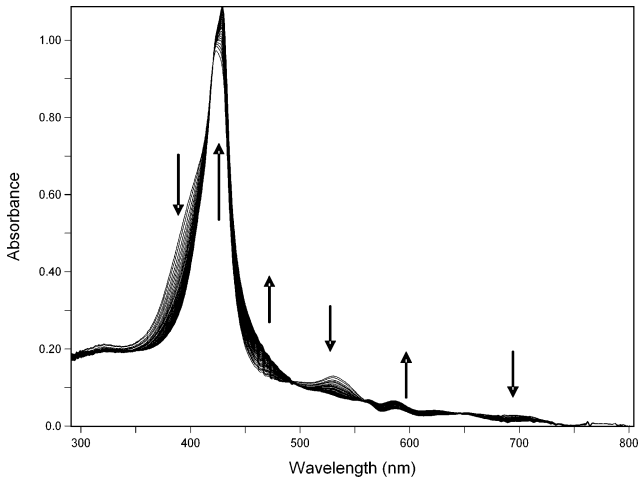

Figure 8. Time-resolved spectra for the reaction between [Fe^{III}(Porph)Cl] and KO_2 at 25 °C in DMSO; [[Fe^{III}(Porph)Cl]] = 5 × 10^{-6} M, [KO_2] = 2.5 × 10^{-5} M.

Infrared Spectroscopy. As in the case of [Fe^{III}(tpp)]$^+$,[8] we could not identify the O−O stretch in the IR spectrum of [Fe^{III}(Porph)(O_2^{2-})]$^-$, prepared by using either $K^{16}O_2$ or $K^{18}O_2$, because a very strong band of [Fe^{III}(Porph)($DMSO)_2$]$^+$ is present (Figure S6, Supporting Information) between 900 and 700 cm^{-1}, which is the region expected for the O−O stretch vibration of a coordinated peroxo ligand. We repeated the IR measurement for [Fe^{III}(tpp)]$^+$, [Fe^{III}(oep)]$^+$, and the corresponding peroxo species (prepared by using KO_2/18-crown-6 according to the reported procedure).[8] Interestingly, we observed that the peak at 806 cm^{-1} with a shoulder at 796 cm^{-1}, which was ascribed to the O−O vibration due to Fe-bound peroxide ligand, is also present in the IR spectrum of KO_2 with 18-crown-6 (Figure S7, Supporting Information), suggesting that this band is due to the ion pair of K^+−crown ether and O_2^-. At the same time, we could not observe any maximum in the IR spectrum of [Fe^{III}(tpp)]$^+$ around 803 cm^{-1} (Figure S8, Supporting Information).[8] This suggests that the band of KO_2/18-crown-6 and not of a porphyrin might be the reason that, in the IR spectrum of [Fe(tpp)(O_2^{2-})] (prepared by using KO_2/18-crown-6), it is not possible to observe the real O−O vibration of coordinated peroxide.

Kinetics and Thermodynamics. Depending on the selected superoxide concentration, two separate reaction steps (Scheme 3) can be studied by the stopped-flow technique. Using less than a 10-fold excess of O_2^- in DMSO at 25 °C or in a mixture of DMSO/CH_3CN at sub-zero temperatures resulted in the same pattern as was observed in the time-resolved spectra, as presented in Figures 8 and S9 (Supporting Information), respectively. The spectrum of the product species is very similar

(38) (a) Horner, O.; Jeandey, C.; Oddou, J.-L.; Bonville, P.; McKenzie, C. J.; Latour, J.-M. *Eur. J. Inorg. Chem.* **2002**, 3278−3283. (b) Simaan, A. J.; Banse, F.; Girerd, J.-J.; Wieghardt, K.; Bill, E. *Inorg. Chem.* **2001**, *40*, 6538−6540.
(39) Horner, O.; Mouesca, J.-M.; Oddou, J.-L.; Jeandey, C.; Niviere, V.; Mattioli, T. A.; Mathe, C.; Fontecave, M.; Maldivi, P.; Bonville, P.; Halfen, J. A.; Latour, J.-M. *Biochemistry* **2004**, *43*, 8815−8825.
(40) Chishiro, T.; Shimazaki, Y.; Tani, F.; Tachi, Y.; Naruta, Y.; Karasawa, S.; Hayami, S.; Maeda, Y. *Angew. Chem., Int. Ed.* **2003**, *42*, 2788−2791.

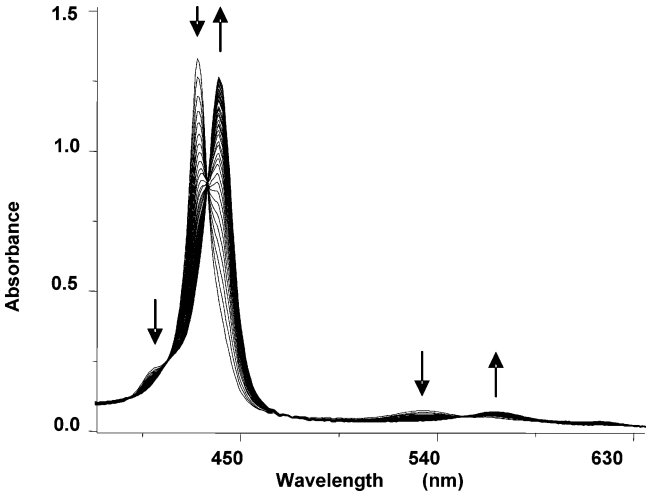

Figure 9. Time-resolved spectra for the reaction between [Fe^{II}(Porph)] and KO_2 at 25 °C in DMSO; [[Fe^{II}(Porph)]] = 5×10^{-6} M, [KO_2] = 5×10^{-4} M.

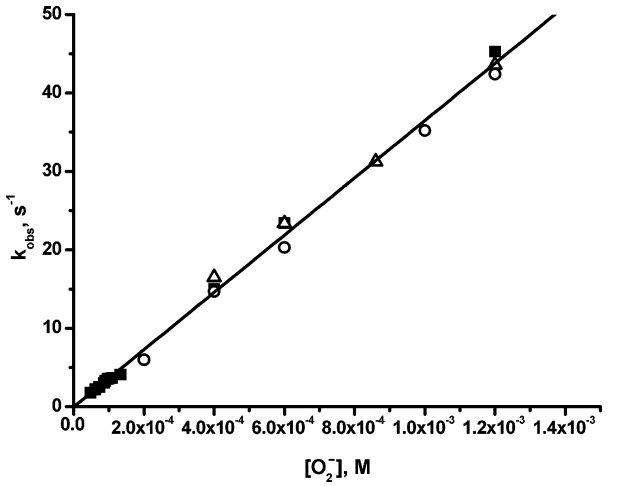

Figure 10. Plots of k_{obs} versus [O_2^-] for the second step of the reaction of 5×10^{-6} M complex and KO_2 at 25 °C in DMSO. Experimental conditions: ■, starting from the Fe(II) complex and using different mixing volume ratios; ○, starting from the Fe(II) complex and preparing a new solution for each [O_2^-]; and △, starting from the Fe(III) complex and preparing a new solution for each [O_2^-].

to that of the Fe(III)−hydroxo complex, with the difference being that the Soret band with a maximum at 430 nm is sharper. The reaction of [Fe^{III}(Porph)$(DMSO)_2$]$^+$ with saturated KOH solution in DMSO led to an almost identical time-resolved spectrum (Figure S10, Supporting Information). The only difference is that the Soret band is broader, which is typical for the hydroxo species. This can be explained by the fact that KO_2 inevitably contains some KOH, which leads to the formation of the Fe(III)−hydroxo complex in a side reaction (Scheme 4). A change in superoxide concentration causes a slight change in k_{obs}, but determination of the second-order rate constant was not attempted because of uncertainties in the KOH concentration.

To check whether the Fe(III)−hydroxo complex is able to react with superoxide, we tested its reaction with a 10-fold excess of O_2^-. The spectrum of the product obtained within 1 s confirms the formation of the Fe(II) complex (Figure S11, Supporting Information, and Scheme 4); moreover, with a slightly higher concentration of O_2^- (achieved by using the variable-mixing-volume-ratio option), the Fe(II) complex that formed within the dead time of the instrument slowly reacted further toward the peroxo species.

The second reaction step (Scheme 3), formation of the Fe(III)−peroxo species, can be monitored in two different ways. When a larger than 10-fold excess of superoxide is applied to the solution of [Fe^{III}(Porph)$(DMSO)_2$]$^+$, the reduced [Fe^{II}(Porph)] complex is formed during the dead time of the instrument, and the formation of the peroxo complex, [Fe^{III}(Porph)(O_2^{2-})]$^-$, is observed. The second reaction step (Scheme 3) can also be followed starting with electrochemically generated [Fe^{II}(Porph)]. All the time-resolved spectra obtained by these two methods were identical, and a typical example is illustrated in Figure 9. Typically, the absorbance maximum at 430 nm decreases while a new band at 440 nm appears. The clear isosbestic points indicate that only one reaction step occurs. The time-resolved spectra can be fitted to a single-exponential function to give values for the observed rate constant, k_{obs}.

Concentration-dependent measurements were performed starting from the Fe(III) complex and also from the electrochemically generated Fe(II) complex. Superoxide concentrations were varied by using the same KO_2 solution and variation of the mixing volume ratios, and also by preparing new solutions for each concentration of KO_2. The results of all these measurements are presented in Figure 10. Although these data were collected by using different starting complexes, viz. Fe(III) and Fe(II) species, respectively, and by applying different methods for varying the superoxide concentration, a very good linear plot of k_{obs} vs [O_2^-] was obtained. This shows that (1) the kinetics of the second step can be studied independently of the first step in the presence of an excess of O_2^- and (2) a good control over the superoxide concentration was achieved in the present study. From the slope of the plot in Figure 10, the second-order rate constant k_{on} was determined to be $36\,500 \pm 500$ M^{-1} s^{-1} (Table 2).

Table 2. Kinetic and Thermodynamic Parameters for Binding of Superoxide to Fe^{II}(Porph) at 25 °C (Second Reaction Step in Scheme 3)

k_{on} (M^{-1} s^{-1})	$36\,500 \pm 500$
k_{off} (s^{-1})	0.21 ± 0.01
$k_{on}/k_{off} = K_{O_2^-}$ [a] (M^{-1})	$(1.7 \pm 0.2) \times 10^5$
$K_{O_2^-}$ [b] (M^{-1})	$(0.9 \pm 0.1) \times 10^5$,[c] $(1.4 \pm 0.1) \times 10^4$ [d]
$\Delta H^{\ddagger}$ (kJ mol^{-1})	61.2 ± 0.9
$\Delta S^{\ddagger}$ (J K^{-1} mol^{-1})	48 ± 3

[a] Kinetically and [b] thermodynamically determined equilibrium constants, [c] with and [d] without electrolyte.

As a result of the large error in the intercept, an accurate value for the rate constant of the back reaction from these experiments could not be estimated. As reported above, addition of a carefully controlled amount of acid, moderate TBPH or strong HOTf, to the green solution of the Fe(III)−peroxo species in DMSO causes its conversion to the Fe(II) complex. Therefore, this reaction, in which acid is a trap for superoxide anions, can be used for direct determination of the rate constant of the back reaction, k_{off}, in a stopped-flow experiment in which a 1×10^{-5} M solution of Fe(III)−peroxo−porphyrin was mixed with the acid solution in DMSO at 25 °C (Figure 4 and Figure S2). It should be mentioned that the high stability of the Fe(III)−peroxo complex enables such an experiment. For the quantitative determination of k_{off}, HOTf was chosen since it is known that strong acids react with superoxide in aprotic solvents extremely rapidly ($k' > 1 \times 10^7$ M^{-1} s^{-1}),[31] which makes them very efficient O_2^- scavengers, even at lower concentrations. The

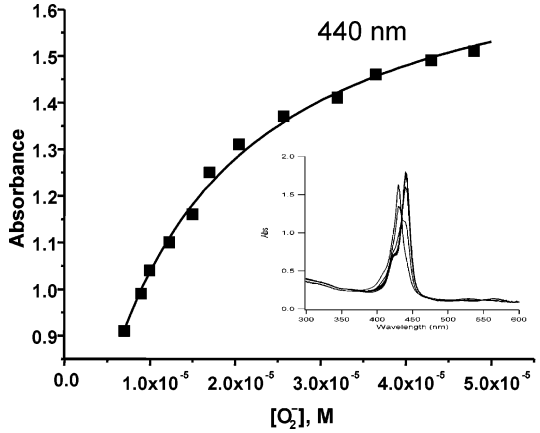

Figure 11. Changes in absorbance at 440 nm upon addition of O_2^- to a 5 $\times$ 10^{-6} M solution of [Fe^{II}(Porph)$(DMSO)_2$] in DMSO at 25.0 °C (I = 0.1 M (NBu_4PF_6)). The solid lines are a fit of the data obtained by global analysis of the resulting spectra (inset) in SPECFIT.

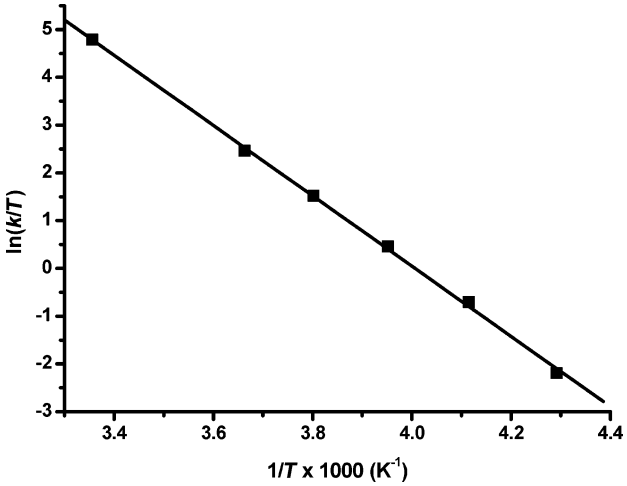

Figure 12. Eyring plot for the second reaction step in the DMSO/CH_3CN mixture (30% DMSO; [[Fe^{III}(Porph)Cl]] = 5 $\times$ 10^{-6} M, [KO_2] = 1 mM).

observed first-order rate constant for the reaction of [Fe^{III}(Porph)(O_2^{2-})]$^-$ and HOTf does not depend on HOTf concentration in the range of 5 $\times$ 10^{-5}–5 $\times$ 10^{-4} M and was found to be $k_{obs} = k_{off} = 0.21 \pm 0.01$ s^{-1} (Table 2). From the obtained second-order rate constant k_{on} and the first-order rate constant k_{off}, the kinetically determined equilibrium constant for the binding of superoxide is $K_{O_2^-} = (1.7 \pm 0.2) \times 10^5$ M^{-1} at 25 °C (Table 2).

The reversible binding of O_2^- to [Fe^{II}(Porph)] and the relative stability of the [Fe^{III}(Porph)(O_2^{2-})]$^-$ complex allowed further investigation of the binding thermodynamics. The equilibrium constant for this reaction was determined by titrating an electrochemically prepared solution of [Fe^{II}(Porph)] with O_2^- under a nitrogen atmosphere. Spectra were recorded about 30 s after addition of the O_2^- aliquot to ensure that the reaction had attained equilibrium. The experiment was performed twice with some variation of the conditions (see Experimental Section), and typical spectra along with the corresponding absorbance changes at 430 and 440 nm are shown in Figure 11. A global analysis of the spectra obtained in two independent experiments (with and without electrolyte) resulted in equilibrium constants for the reaction of (0.9 $\pm$ 0.1) $\times$ 10^5 and (1.4 $\pm$ 0.1) $\times$ 10^4 M^{-1} (Table 2), respectively, which is within the expected trend for ion-pair formation constants as a function of ionic strength. Thus, both thermodynamically and kinetically determined equilibrium constants for superoxide binding are in good agreement.

Starting from the [Fe^{III}(Porph)$(DMSO)_2$]$^+$ complex and applying high enough [O_2^-], the second reaction step (Scheme 3) was studied as a function of temperature (−40 to 0 °C) in a DMSO/CH_3CN mixture (30% DMSO with the lowest freezing point about −50 °C). The k_{on} (= k_{obs}/[O_2^-]) values obtained in the DMSO/CH_3CN mixture at low temperatures are in very good agreement with the second-order rate constant obtained in DMSO solution at 25 °C (Figure 12, Table 2, Table S1, Supporting Information). This is indicated by a very good linear correlation between ln(k_{on}/T) and 1/T over a wide temperature range (−40 to +25 °C) (Figure 12 and Table S1). Coordination of DMSO to Fe(III)−porphyrin−peroxo complexes already occurs in the presence of 20% DMSO in CH_3CN, resulting in a bis-axially coordinated species.[13] This observation, together with the comparative kinetic behavior of the studied reaction

Scheme 5

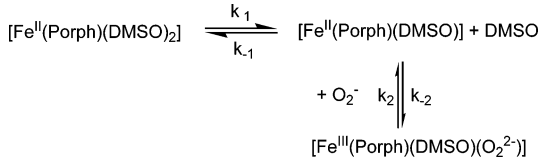

in pure DMSO and DMSO/CH_3CN mixtures, suggests that in both solutions the same reacting bis-DMSO−Fe(III) species exists. Thus, the reactions and the corresponding rate constants in pure DMSO and DMSO/CH_3CN mixtures are fully comparable.

The activation parameters resulting from the temperature-dependent measurements of k_{on} were found to be $\Delta H^{\ddagger} = 61.2 \pm 0.9$ kJ mol^{-1} and $\Delta S^{\ddagger} = +48 \pm 3$ J K^{-1} mol^{-1} (Table 2). The relatively high value of the activation enthalpy and a positive value of the activation entropy speak for a dissociative mode of the second reaction step (Scheme 3), in which the redox process is substitution controlled. Dissociation of coordinated DMSO from the six-coordinate [Fe^{II}(Porph)$(DMSO)_2$] complex (a D mechanism, Scheme 5), resulting in the five-coordinate intermediate, is suggested to be the rate-determining step. This is also in agreement with the strong coordinating ability of DMSO. In a limiting dissociative D mechanism according to eq 3, a kinetic saturation behavior is expected, where k_1 and

$$k_{obs} = \frac{k_1 k_2 [O_2^-] + k_{-1} k_{-2}}{k_{-1} + k_2 [O_2^-]} \qquad (3)$$

k_{-1} are the forward and reverse rate constants for the dissociation of DMSO, and k_2 and k_{-2} are the forward and reverse rate constants for the coordination of O_2^-. However, under the selected experimental conditions, k_2[O_2^-] is much smaller than k_{-1}, such that eq 3 can be simplified to $k_{obs} = k_{on}$[O_2^-] + k_{off}, with the overall second-order rate constant for superoxide binding $k_{on} = k_1 k_2 / k_{-1}$ and the first-order rate constant for the superoxide release $k_{off} = k_{-2}$. Looking at eq 3, the linear concentration dependence of k_{obs} can easily be understood since superoxide is present in a much lower concentration than DMSO to scavenge the five-coordinate intermediate, such that k_2[O_2^-] in eq 3 is negligible in comparison to k_{-1}. Thus, the activation parameters obtained involve contributions from the effect of

Scheme 6

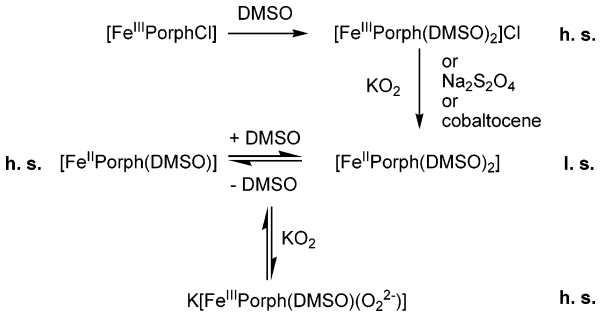

temperature on the formation of the five-coordinate intermediate ($\Delta H(K_1)$ and $\Delta S(K_1)$) and on the rate of superoxide binding, k_2 ($\Delta H^{\ddagger}(k_2)$ and $\Delta S^{\ddagger}(k_2)$). In this case, there is a combination of two opposite effects, which explains the rather moderate positive value obtained for $\Delta S^{\ddagger}$.

Conclusions

We have synthesized and characterized the new Fe(III)−porphyrin complex [Fe^{III}(Porph)Cl], which carries a covalently bound aza-crown ether in close proximity to the iron center. The corresponding hydroxo, μ-oxo dimer, Fe(II), and Fe(III)−peroxo species were also prepared. The quite high stability of the Fe(II)−porphyrin and Fe(III)−peroxo−porphyrin species enabled kinetic and thermodynamic measurements to be made for the reaction with KO_2 in DMSO. As mentioned above, in contrast to the Fe(III)−peroxo−porphyrin species reported in the literature,[10] which are only stable under an inert atmosphere, our peroxo species is quite stable in solution with an excess of superoxide, even when exposed to air. The presence of nearby K^+ can account for this increased stability of K[Fe^{III}(Porph)-(O_2^{2-})].

The reactions studied are summarized in Scheme 6. The first reaction step, reduction of the Fe(III) to the Fe(II)−porphyrin complex by KO_2, could not be studied in detail because of interference from the formation of the Fe(III)−hydroxo species. The second reaction step, binding of superoxide to the Fe(II) species and formation of the Fe(III)−peroxo complex, could be studied in detail. To our knowledge, this is the first time that superoxide concentration and temperature-dependent kinetic studies of reactions with superoxide have been performed by stopped-flow UV/vis measurements, and as a result the second-order rate constant and corresponding activation parameters could be obtained. Moreover, we have observed for the first time that the superoxide anion can bind reversibly to a metal center. We have determined the rate constant for the reverse reaction as well as measured kinetic and thermodynamic superoxide binding constants.

On the basis of the results obtained, we can conclude that strongly coordinated DMSO controls the reaction mechanism in the sense that its dissociation is the rate-determining step. We have also shown that addition of acid (or proton sources in general) to the Fe(III)−peroxo species does not necessarily lead to dissociation of hydrogen peroxide and formation of the Fe(III) complex (as in the case of the SOD active enzymatic and mimetic systems)[6,7] or O−O bond cleavage and formation of a high-valent oxo−iron species (as in the case of cytochrome P450). Specifically, we have shown that, if the Fe(III)−peroxo species is in equilibrium with superoxide, fine-tuning of the proton concentration can lead to superoxide trapping and formation of an Fe(II) species. Whether this type of reactivity is a result of the unique structural feature of our Fe(III)−peroxo−porphyrin (viz. the presence of the nearby K^+−crown ether moiety) or a more general feature that could not be observed before because of the much lower stability of the previously studied Fe(III)−peroxo−porphyrin complexes remains to be seen. This also stresses the possible effect of the electrostatic interactions between the coordinated peroxide and the positively charged surrounding groups, as well as the effect of the axially coordinated group, on the stability of the peroxo species and molecular mechanism of O−O bond cleavage. In any case, this type of reactivity of the Fe(III)−peroxo species and reversible binding of superoxide could be of significant biological importance since it could operate in a specific biological environment as well.

Chart 1

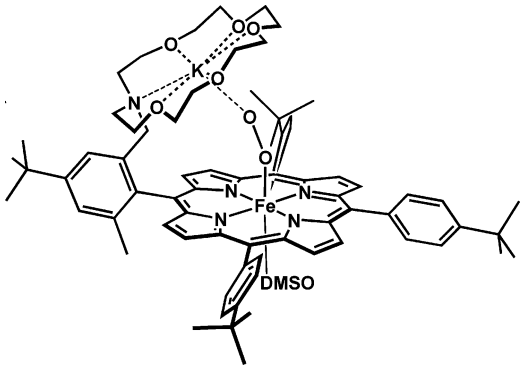

It is not possible to conclude whether the peroxo ligand in our [Fe^{III}(Porph)(O_2^{2-})]$^-$ complex is coordinated in a side-on or end-on fashion. However, with coordinated DMSO and the electrophilic potassium cation in the crown ether lying above the peroxo ligand, [Fe^{III}(Porph)(O_2^{2-})]$^-$ may in a way represent a model for the proposed[13] nucleophilic attack of the end-on peroxo form, with an axially coordinated solvent molecule, to an electron-deficient substrate (see Chart 1).

Similar studies on the related Mn(III) complex of our crown ether−porphyrin conjugate, as well as on the corresponding Fe(III) and Mn(III) complexes of the porphyrin ligand without a crown ether moiety, are in progress.

Acknowledgment. The authors gratefully acknowledge financial support from the Deutsche Forschungsgemeinschaft through SFB 583 "Redox-active metal complexes" (I.I.-B. and N.J.).

Supporting Information Available: UV/vis spectra of different species, time-resolved UV/vis spectra of different reaction steps, IR spectra, and results of the electrochemical studies (PDF); crystallographic data for {[Fe^{III}(Porph)Cl]·H_3O^+}$FeCl_4^-$ (CIF; also deposited with the Cambridge Crystallographic Data Centre as CCDC 612689). This material is available free of charge via the Internet at http://pubs.acs.org.

JA064984P